Water Research 270 (2025) 122809

Contents lists available at ScienceDirect

Water Research

journal homepage: www.elsevier.com/locate/watres

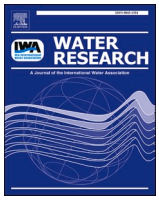

Influence of filter backwashing on iron, manganese, and ammonium removal in dual-media rapid sand filters used for drinking water production

Alje S. Boersma [a], Signe Haukelidsaeter [b], Liam Kirwan [b], Alessia Corbetta [b], Luuk Vos [c], Wytze K. Lenstra [a,b], Frank Schoonenberg [d], Karl Borger [d], Paul W.J.J. van der Wielen [c,e], Maartje A.H.J. van Kessel [a], Caroline P. Slomp [a,b], Sebastian Lücker [a,*]

[a] Department of Microbiology, RIBES, Faculty of Science, Radboud University Nijmegen, P.O. Box 9010, Nijmegen, GL 6500, The Netherlands
[b] Department of Earth Sciences, Faculty of Geosciences, Utrecht University, P.O Box 80021, 3508 TA Utrecht, The Netherlands
[c] KWR Water Research Institute, P.O. Box 1072, Nieuwegein, BB 3430, The Netherlands
[d] Vitens N.V., P.O. Box 1205, Zwolle, BE 8001, The Netherlands
[e] Laboratory of Microbiology, Wageningen University & Research, Stippeneng 4, WE 6708, Wageningen, The Netherlands

ARTICLE INFO

Dataset link: BioProject PRJNA1107137 (Original data) https://www.ncbi.nlm.nih.gov/bioproject/?term=PRJNA1107137

Keywords:
Gallionella
Nitrification
Rapid sand filter
Drinking water production
Filter backwashing

ABSTRACT

Iron (Fe), manganese (Mn), and ammonium (NH_4^+) removal from groundwater using rapid sand filtration is a widely employed method in drinking water production. Over time, Fe and Mn oxides accumulate in the filter, which necessitates frequent backwashing to avoid clogging. In this study, we investigated the impact of backwashing on the microbial community and filter chemistry in a dual-media filter comprising anthracite and sand layers. Specifically, we focused on the removal of Fe, Mn, and NH_4^+ over the runtime of the filter. With increasing runtime, depth profiles of dissolved and particulate Fe revealed the buildup of Fe oxide flocs, causing Fe^{2+} and Mn^{2+} oxidation and nitrification to occur at greater depths within the filter. Towards the end of the filter runtime, breakthrough of suspended Fe oxides was observed, likely due to preferential flow. Backwashing effectively removed metal oxide flocs and restored the Fe removal efficiency in the top layer of the filter. While the two layers remained separate, the anthracite and sand layers themselves fully mixed during backwashing, leading to a homogenous distribution of the microbial community within each layer. *Methyloglobulus* and *Gallionella* were the predominant organisms in the anthracite layer, likely catalyzing methane and Fe^{2+} oxidation, respectively. The nitrifying community of the anthracite consisted of *Nitrosomonas, Candidatus* Nitrotoga, and *Nitrospira*. In contrast, the nitrifying community in the sand layer was dominated by *Nitrospira*. Backwashing minimally affected the microbial community composition of the filter medium except for *Gallionella*, which were preferentially washed out. In conclusion, our research offers a molecular and geochemical basis for understanding how backwashing influences the performance of rapid sand filters.

1. Introduction

Groundwater accounts for 97% of the global freshwater supply, excluding glaciers and icecaps, and is the source of almost half of all drinking water in the world (van der Gun, 2012). Before anoxic groundwater can be used as drinking water, methane (CH_4), iron (Fe), manganese (Mn), and ammonium (NH_4^+) need to be removed due to their potentially toxic nature and the risk of bacterial regrowth or fouling in the distribution system. Aeration followed by rapid sand filtration is a commonly employed method to achieve their removal, where CH_4 is stripped and Fe, Mn, and NH_4^+ are oxidized and removed in the filter.

Fe and Mn can be removed by biological and chemical processes, with either homogeneous or heterogeneous chemical oxidation for the latter. In the case of heterogeneous oxidation, dissolved Fe^{2+} and Mn^{2+} adsorb onto mineral coatings composed of metal oxides on the filter medium, where they undergo hydrolysis and oxidation (van Beek et al., 2016; Vries et al., 2017). Under the pH conditions at which rapid sand filters operate, homogeneous oxidation occurs only for Fe, leading to the formation of Fe oxide flocs (van Beek et al., 2016). The biological oxidation of Fe^{2+} in rapid sand filters is often catalyzed by *Gallionella* spp. (de Vet et al., 2011; Gülay et al., 2018; van Beek et al., 2016) and

* Corresponding author.
E-mail address: s.luecker@science.ru.nl (S. Lücker).

https://doi.org/10.1016/j.watres.2024.122809
Received 22 April 2024; Received in revised form 14 November 2024; Accepted 16 November 2024
Available online 17 November 2024

Leptothrix spp., which, however, may depend on dissolved organic carbon (DOC) to grow hetero- or mixotrophically (Fleming et al., 2018). Other bacteria, such as diverse members of the *Acidivorax, Burkholderiales, Ferriphaselus, Undibacterium*, and *Curvibacter* are found at low abundances in rapid sand filters and might contribute to Fe removal (Gülay et al., 2013, 2018). Biological Fe^{2+} oxidation is generally thought to be favored at slightly acidic pH (6.5–7.0) and low oxygen (O_2) concentrations (< 6 mg L^{-1}) (van Beek et al., 2016; Vries et al., 2017; Müller et al., 2024). However, also in groundwater with higher pH (7.5–8.0), chemical and biological Fe^{2+} oxidation may co-occur, as low temperatures typical for groundwater in moderate and colder climates might slow chemical oxidation rates (Sung and Morgan, 1980; Gülay et al., 2013). The bacteria involved in Mn^{2+} oxidation are not well recognized, with various genera proposed to be involved. For instance, *Pseudomonas* spp. have been linked to Mn^{2+} oxidation in rapid sand filters through both culture-dependent and independent methods (Bruins et al., 2017; Hu et al., 2020; Marcus et al., 2017). Metagenome-assembled genomes of bacteria belonging to the *Burkholderiales* and *Rhizobiales* contain proteins putatively involved in Mn^{2+} oxidation (Palomo et al., 2016), and the rhizobial genera *Pedomicrobium* and *Hyphomicrobium* have been hypothesized to contribute to Mn^{2+} removal based on their high abundances in rapid sand filters (Larsen et al., 1999; Albers et al., 2014; Palermo and Dittrich, 2016).

In contrast to Fe and Mn, NH_4^+ is only removed by biological processes. Oxidation of ammonia (NH_3) to nitrite (NO_2^-) and subsequently nitrate (NO_3^-) can be performed in a two-step process by ammonia-oxidizing bacteria or archaea in conjunction with nitrite-oxidizing bacteria, or by *Nitrospira* able to perform complete ammonia oxidation (comammox) (Daims et al., 2015; Van Kessel et al., 2015). Rapid sand filters typically have a higher abundance of *Nitrospira* compared to other nitrifiers (Albers et al., 2014; Gülay et al., 2016) and metagenomics-based approaches revealed the presence of comammox *Nitrospira* in rapid sand filters (Palomo et al., 2016; Poghosyan et al., 2020), indicating their ability to perform complete ammonia oxidation to be the reason for their high abundances. Recent findings show that within the initial eight months following filter replacement, *Nitrosomonas* and *Candidatus* Nitrotoga were the dominant nitrifiers before the later proliferation of *Nitrospira*, indicating a succession of different nitrifiers after filter replacement that is likely defined by their individual growth rates (Haukelidsaeter et al., 2023).

The microbial communities in the incoming groundwater and the rapid sand filters used to treat the groundwater are usually distinct (Nitzsche et al., 2015; Gülay et al., 2016). A determining factor in this change in community composition is likely the shift in dissolved oxygen levels from typically anoxic in the groundwater to (super-)saturated after the aeration step of the treatment (Gülay et al., 2016).

With increasing operation time between backwash cycles, the filter bed resistance of rapid sand filters increases (Bourke et al., 1995). This is mainly the result of an accumulation of Fe oxide flocs due to the high O_2 and rise in pH in the supernatant water (Vries et al., 2017; Gude et al., 2018; Haukelidsaeter et al., 2024), which is known to hinder NH_4^+ removal in full-scale sand filters as well as pilot-scale columns (Corbera-Rubio et al., 2024; De Vet et al., 2009). To restore proper filter function, regular backwashing is necessary. The frequency of backwashing is largely dependent on the Fe loading of the filter and in primary filters typically occurs every 1–4 days, using a reverse flow of water and/or air through the filter (Ramsay et al., 2021; Beshr et al., 2023). While backwashing is a common practice in the operation of rapid sand filters, its effects on the microbial community and removal processes of solutes in the filter are not well understood. Characteristic stalks of *Gallionella* have been identified in backwash sludge, suggesting some level of microbial community alteration in the filter (van Beek et al., 2012; Müller et al., 2024). In a single media filter, stratification of the microbial community despite backwashing has been reported (Haukelidsaeter et al., 2024). Furthermore, backwashing may cause partial loss of the mineral coating on filter grains (van Beek et al., 2016). However, this coating removal cannot exceed the development rate, considering the increased thickness of mineral coatings observed in older filters (Haukelidsaeter et al., 2023). Lastly, in dual-media rapid sand filters, which consist of a layer of anthracite coal above the sand layer to better retain and remove particulate impurities like Fe oxide flocs, the two layers can mix (Ramsay et al., 2021), but usually remain separated after backwashing (Corbera-Rubio et al., 2023). However, the effect of backwashing on microbial community mixing within the different layers has not been studied in high resolution in dual-media filters.

It is important to study the impact of backwashing on the microbial community and filter performance in diverse locations due to the significant variability in groundwater chemistry and operating conditions. The objective of our study was to expand the current understanding of how backwashing impacts dual-media rapid sand filters used for treating groundwater with high concentrations Fe^{2+}, Mn^{2+}, and especially NH_4^+, at a full-scale drinking water treatment plant. Specifically, we focused on the effects of Fe floc accumulation on the removal of these compounds, as well as the influence of backwashing on the microbial community and the mineral coating.

2. Materials and methods

2.1. Drinking water treatment plant

Samples were collected from the Vitens N.V. Drinking Water Treatment Plant (DWTP) located in Sint Jansklooster, the Netherlands (52°40′41.2″N 6°00′47.8″E). The chemical composition of the raw water at this site fluctuates across the 18 wells from which groundwater is extracted. Generally, the Fe concentration varies between approximately 125–180 μM, Mn between 6 and 8 μM, and NH_4^+ levels between approximately 70–200 μM. The temperature typically is within the range of 11–12 °C.

The treatment process at the Sint Jansklooster DWTP involves 11 distinct steps (Supplementary Figure S1), as outlined in detail by Haukelidsaeter et al. (2024). Following plate aeration, raw water is distributed across 12 parallel dual-media filters, each covering an area of 25 m^2. These filters consist of layers of approximately 0.9 m of anthracite (particle size: ⌀ 1.4–2.5 mm) and 1.6 m of sand (⌀ 0.8–1.2 mm), with porosities of approximately 50% and 42%, respectively. The supernatant level on top of the filters has an average height of approximately 0.1 m. In this study, we specifically sampled pre-filter 11 (VF11) for analysis, of which the anthracite and sand layers were replaced in 2019 and 2010, respectively. Notably, before the most recent sampling, additional O_2 dosing was introduced to the influent. This was done by evaporating pure O_2 gas under atmospheric conditions in the influent water before it was distributed across all filters.

At the Sint Jansklooster DWTP, the filters are typically backwashed after approximately 7000 m^3 of water have passed through (equivalent to 112 empty bed volumes), which occurs on average over a period of 3 to 4 days. The backwash procedure uses approximately 200 m^3 of prefiltrate water (i.e., the effluent water from the primary rapid sand filtration step) and is performed according to the following sequence: a 3-minute water wash at a rate of 1500 $m^3\ h^{-1}$, followed by a 2-minute water wash with decreasing flow from 1500 to 0 $m^3\ h^{-1}$, a 5-minute air scour at a rate of 60 $Nm^3\ m^{-2}\ h^{-1}$, a 4-minute water wash at 1500 $m^3\ h^{-1}$, and finally, a 1-minute 40-second water wash with decreasing flow from 1500 to 0 $m^3\ h^{-1}$.

2.2. Sample collection

Samples were collected in March, June, and October 2021. In March, samples were obtained after the filter had been running for 72 h (just before backwashing), and 2 h and 24 h after backwashing. In June, samples were taken after the filter had been running for 136 h (just before backwashing) and 2 h after backwashing. In October, samples

were collected after 48 h of filter runtime (1 h before backwash), as well as 2 h and 24 h after the backwash. Single samples were taken during all collections. For the March and October samples, the Fe and Mn load was calculated from the influent solute concentrations and the volumes of filtered water (Table 1). The hydraulic loading rate (HLR) of water within the filter under investigation was estimated based on the overall HLR of six parallel filters, as the water from the preceding treatment step was evenly distributed among these six filters. During the March sampling, the HLR was not consistent and changed from 24 $m^3\ m^{-2}\ h^{-1}$ before to 12.8 $m^3\ m^{-2}\ h^{-1}$ right after backwashing, and to 11.4 $m^3\ m^{-2}\ h^{-1}$ after one day of operation. In October 2021, this issue was resolved and the HLR was 15.2 $m^3\ m^{-2}\ h^{-1}$ during all three sampling times.

Abstracted groundwater samples were collected from a tap prior to plate aeration. Filter influent samples were collected directly from the top of the filter (i.e., supernatant water). To assess where Fe, Mn, and NH_4^+ were removed in the filter, water samples were obtained from 11 taps at different depths of the filter (every 20 cm), as well as the filter effluent. Filtered (0.45 μM, Nylon syringe filter, Genetec) water samples for determination of dissolved Fe and Mn were collected in 15-mL Greiner tubes and acidified with ultra-pure nitric acid (HNO_3, 10 μL per 1 mL sample) upon arrival at the laboratory. Filtered water samples for the analysis of NH_4^+, NO_2^-, and NO_3^- were stored at −20 °C. In March 2021, water samples for CH_4 were collected from the raw water and supernatant in 125-mL serum bottles by allowing the water to overflow, ensuring no air bubbles were introduced. The bottles were immediately sealed with butyl rubber stoppers and secured with aluminum crimp caps. To preserve the samples, 1 mL of saturated $ZnCl_2$ solution was added to each bottle. The samples were stored inverted in the dark to prevent contamination and degradation.

In March 2021, samples of anthracite and sand were collected for Fe and Mn oxide determination. A stainless-steel peat sampler (Veenlans 04.09, Royal Eijkelkamp, Giesbeek, The Netherlands) was used to collect samples from up to 2 m deep within the filter. Anthracite samples were collected at various depth intervals (15 samples in total: 0–2 cm, 2–4 cm, 4–6 cm, 6–8 cm, 8–10 cm, 10–15 cm, 15–20 cm, 20–25 cm, 25–30 cm, 30–40 cm, 40–50 cm, 50–60 cm, 60–70 cm, 70–80 cm, and 80–90 cm). Similarly, sand samples were collected at eight depth intervals, with each interval representing a depth of 10 cm. These samples were stored in 50-mL Greiner tubes at −20 °C.

In June 2021, raw water, effluent water at 136 h and 2 h of filter runtime, and backwash water samples were taken for microbial community analysis. Backwash water samples were collected every minute during the water washing stages of the backwash procedure. This resulted in four backwash water samples during the initial and five samples during the subsequent water washing period. Between these two washing steps, the filter was allowed to settle and air-scoured for five minutes (see above for the backwashing procedure).

For microbial community analysis of the filter medium, seven samples were collected in March and June 2021 from the anthracite (depth intervals: 0–4 cm, 4–10 cm, 10–15 cm, 15–20 cm, 25–30 cm, 30–50 cm, 50–100 cm), and two samples from the sand (depth intervals: 100–150 cm, 150–200 cm). Each filter medium sample was prepared by collecting equal amounts of material throughout the depth interval, and then manually mixing by shaking the material in 50-mL Greiner tubes. All samples were taken from a single horizontal location in the filter and stored at −20 °C until DNA isolation.

Table 1
Fe and Mn load to the filter during one filter run, as calculated from influent concentrations and the volume of filtered water.

Sampling	Runtime	Water filtered (m^3)	Fe load (kg)	Mn load (kg)
March 2021	72 h	4600	34	1.58
	2 h	93	0.7	0.03
	24 h	1080	9	0.4
October 2021	48 h	5800	43	2.07
	2 h	90	0.9	0.04
	24 h	1140	11	0.5

2.3. Water chemistry analysis

Water pH, O_2 concentration, conductivity, and temperature were measured on-site in overflowing plastic bottles using a HQ40D Portable Multimeter (HACH, Düsseldorf, Germany). Particulate and dissolved Fe and Mn were analyzed using a Perkin-Elmer Avio 500 Inductively Coupled Plasma Optical Emission Spectrophotometer (ICP-OES; detection limit (LOD) Fe = 0.023 mg L^{-1} or 0.4 μM, Mn = 0.001 mg L^{-1} or 0.02 μM). The concentration of NH_4^+, NO_2^-, and NO_3^- (LOD NH_4^+ = 0.3 μM, NO_2^- = 0.02 μM, NO_3^- = 0.09 μM) in the filtered water samples was determined spectrophotometrically with a Thermo Scientific™ Gallery Analyzer. The measurement of NOx followed the methodology described in Jumppanen et al. (2014), while NH_4^+ was measured according to the ISO7150–1:1984 standard. To determine the CH_4 concentrations, 5 mL of nitrogen gas was added to each sample, removing an equivalent volume of liquid. CH_4 concentrations were measured using a Thermo Finnigan Trace™ gas chromatograph equipped with a Flame Ionization Detector, with a detection limit of 0.02 μmol L^{-1}, following gas and water phase equilibration for >2 h.

The turbidity in the effluent of VF11 was determined by Vitens N.V. using a CUS52D Turbidimeter (Endress+Hauser, Reinach BL, Switzerland) continuous turbidity sensor (installed in November 2022). Turbidity data was analyzed from a backwash sequence starting 5th of January until 9th of January 2023 while the filters were operated in a similar manner to the sampling times in 2021.

2.4. Geochemical filter medium analysis

The amount of Fe and Mn oxides present in the filter material coating was determined using a two-step sequential extraction procedure with ascorbic acid and HCl (Claff et al., 2010; Lenstra et al., 2021). The filter medium was first oven-dried at 60 °C for 20 h. Subsequently, 100–250 mg filter medium was mixed with 10 ml extractant in two separate steps. All samples were measured with ICP-OES as described above.

Scanning Electron Microscopy (SEM) was used for elemental mapping and high-resolution imaging of backwash sludge characteristics. Selected filter media samples were freeze-dried and fixed to 0.5-inch aluminum SEM specimen stubs (Agar Scientific Ltd.) using carbon adhesive discs. Mounted samples were coated with 10 nm of platinum using a sputter coater (208HR Sputter Coater, Cressington). Backscattered electron images were acquired with Zeiss Evo 15 SEM, equipped with EDS for element mapping.

2.5. DNA isolation and 16S rRNA gene amplicon sequencing

DNA was extracted from 0.5 g (wet weight) filter material using the DNeasy Powersoil DNA isolation kit (QIAGEN, Hilden, Germany), with minor modifications. Cell lysis was performed by bead beating at 50 Hz for 1 min using a TissueLyser LT (QIAGEN, Hilden, Germany). When insufficient DNA concentrations were obtained from these extractions, up to four cell lysis replicates using 0.5 g sample material each were pooled on one GeneJet Spin column. Finally, DNA was eluted in 100 μL DEPC water, with a 1 min incubation step at room temperature of the silica matrix in the DEPC water prior to the final centrifugation. From water samples, DNA was extracted using the DNeast Powerwater DNA isolation kit (QIAGEN, Hilden, Germany). For effluent and influent water, 1 L was used, and 50 ml for backwash water samples. The samples were concentrated on a 0.2 μm nylon filter (⌀ 47 mm; Pall Corporation, Port Washington, USA), which was then washed with 10 mL 0.5 M ammonium oxalate (pH 3), and subsequently with 10 mL 1 × phosphate buffer saline (PBS). DNA was eluted in 50 mL DEPC water, using a 1 min incubation step as described above.

16S rRNA gene amplicon sequencing was performed by Macrogen Inc. (Seoul, South Korea) using the Illumina MiSeq platform. Primers used for bacterial 16S rRNA gene amplification were 341F (5′-CCTACGGGNGGCWGCAG-3′; Herlemann et al., 2011) and 806R (5′-GGACTACHVGGGTWTCTAAT-3′; Caporaso et al., 2012). Paired-end libraries were constructed using the Herculase II Fusion DNA Polymerase Nextera XT Index Kit V2 (Illumina, San Diego, USA) with the 16S Metagenomic Sequencing Library Preparation Part # 15,044,223 Rev. B protocol. On average 106,059 (*SD* = 13,670) paired end reads were obtained per sample. The data was processed in R (v3.5.1; R Core Team, 2019) using the DADA2 pipeline (v1.8; Callahan et al., 2016). The 16S rRNA gene-based taxonomy was obtained using the SILVA database (release 138.1, Quast et al., 2013). The relative abundances as calculated using DADA2 were analyzed using the R package Phyloseq (v1.30.0; McMurdie and Holmes, 2013).

2.6. Quantitative PCR

Bacterial 16S rRNA gene copy numbers were determined by qPCR as previously described (Haukelidsaeter et al., 2023) using the primers 331F (5′-TCCTACGGGAGGCAGCAGT-3′, Nadkarni et al., 2002) and 518R (5′-ATTACCGCGGCTGCTGG-3′, Muyzer et al., 1993). PCR reactions were performed in a C1000 Touch thermocycler with a CFX96 Touch real-time detection system (Bio-Rad Laboratories B.V., Veenendaal, The Netherlands) with the following program: initial denaturation at 95 °C for 5 min, 44 cycles of denaturation at 95 °C for 30 s, annealing at 60 °C for 30 s, and elongation at 72 °C for 45 s, and a final elongation step at 72 °C for 10 min. This was followed by a final denaturation at 95 °C for 10 s, followed by a melting curve preparation at 65 °C for 1 min, and a melting curve analysis from 65 to 95 °C, with 0.5 °C increments every 5 s.

3. Results & discussion

3.1. Chemical and microbial characteristics of the filter

At the time of sampling, oxygen was always present in the filter (> 112 μM) and the pH was near neutral (7.4–7.2; Supplementary data). Most CH_4 was effectively stripped during plate aeration, reducing its concentration from an average of 201 μM in the raw water to 1.4 μM in the supernatant (Supplementary Data). Fe was primarily removed in the anthracite layer and was present in both dissolved and particulate forms. In contrast, Mn was primarily present as dissolved Mn^{2+} and was mostly removed in the sand layer. Still, removal was only 80% complete, and ~1–2 μM of Mn leaked through to the filter effluent (Fig. 1). All NH_4^+ was oxidized to NO_3^-, with NO_2^- accumulating to 0.1–0.3 μM in the anthracite layer (Figure 2; Supplementary data). The decrease in O_2 and NH_4^+ concentrations followed the same pattern (Fig. 2) with a ratio close to 2:1, indicating that nitrification is the main driver of O_2 removal. Before and after the introduction of additional O_2 dosing, which increased supernatant O_2 concentrations from an average of 319 μM to 407 μM, the entire filter remained oxic, with effluent O_2 concentrations averaging 130 μM and 168 μM before and after dosing, respectively (Supplementary Data). Given the similar removal profiles observed before and after dosing (Fig. 1) and the sustained oxic conditions, we conclude that the O_2 dosing did not affect filter performance at the time of sampling.

The depths of Fe and Mn^{2+} removal were reflected in the composition of the mineral coating, which on the anthracite consisted mostly of

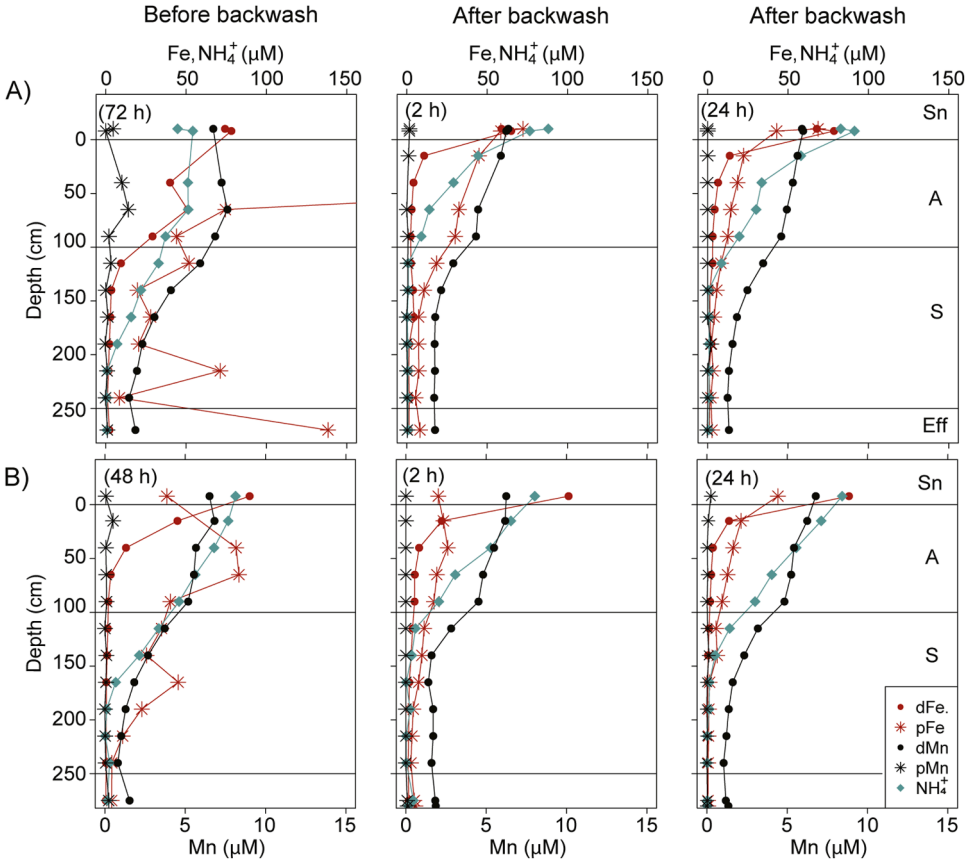

Fig. 1. Removal profiles of Fe, Mn, and NH_4^+ throughout the filter. Concentrations of dissolved Fe (red dots), particulate Fe (red stars), dissolved Mn (black dots), particulate Mn (black stars), and NH_4^+ (green diamonds) with depth in the filter. Profiles for (A) March 2021 were taken 72 h (4600 m^3 water filtered and a HLR of 24 $m^3\ m^{-2}\ h^{-1}$), 2 h (93 m^3 and 12.8 $m^3\ m^{-2}\ h^{-1}$) and 24 h (1080 m^3 and 11.4 $m^3\ m^{-2}\ h^{-1}$) after backwashing, and (B) October 2021 at 48 h (5800 m^3 and 15.2 $m^3\ m^{-2}\ h^{-1}$), 2 h (120 m^3 and 15.2 $m^3\ m^{-2}\ h^{-1}$) and 24 h (1140 m^3 and 15.2 $m^3\ m^{-2}\ h^{-1}$) after backwashing. Sn, Supernatant; A, Anthracite; S, Sand; Eff, Effluent.

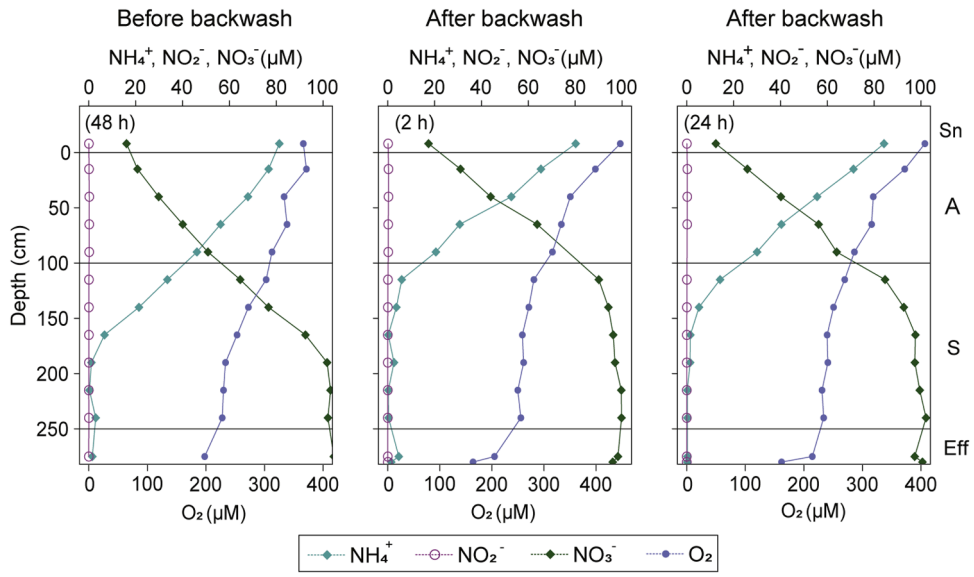

Fig. 2. Removal profiles of NH_4^+, NO_2^-, and NO_3^- throughout the filter. Concentrations of NH_4^+ (light green diamonds), O_2 (blue dots), NO_2^- (purple open circles), and NO_3^- (dark green diamonds) with depth in the filter. Samples were obtained in October 2021 at 48 h, 2 h, and 24 h after backwash. Sn, Supernatant A, Anthracite; S, Sand; Eff, Effluent.

Fe oxides, while a combination of Mn and Fe oxides comprised the coating on the sand grains (Supplementary Figure S2). All Fe and Mn oxides were easily soluble and of poor crystallinity, as was previously confirmed by X-ray diffraction (Haukelidsaeter et al., 2023). The incomplete removal of Mn in the filter could be explained by its age, as Mn removal efficiency declines in older filters with thick mineral coatings (Haukelidsaeter et al., 2023).

The microbial community of the filter medium was found to be comparable across the different sampling depths of each media type, but distinct between the anthracite and sand layers, as also was observed previously (Haukelidsaeter et al., 2023). While shifts in relative abundances were observed between the microbial communities present in the March (Supplementary Figure S3) and June (Fig. 3) samples, the overall community structure remained highly similar. The presumably methane-oxidizing members of the *Methylomonadaceae* (25–32% relative abundance) and functionally distinct microorganisms within the *Gallionellaceae* (6–13%) were the most abundant families in the anthracite layer (Fig. 3 and Supplementary Figure S3). The *Methylomonadaceae* consisted mostly of the genus *Methyloglobulus* (82–92%), while the *Gallionellaceae* comprised the iron-oxidizing genus *Gallionella* (72–78%; Table 2 and Supplementary Table S1) and the nitrite-oxidizing *Candidatus* Nitrotoga (18–25%). In addition to *Candidatus* Nitrotoga, the

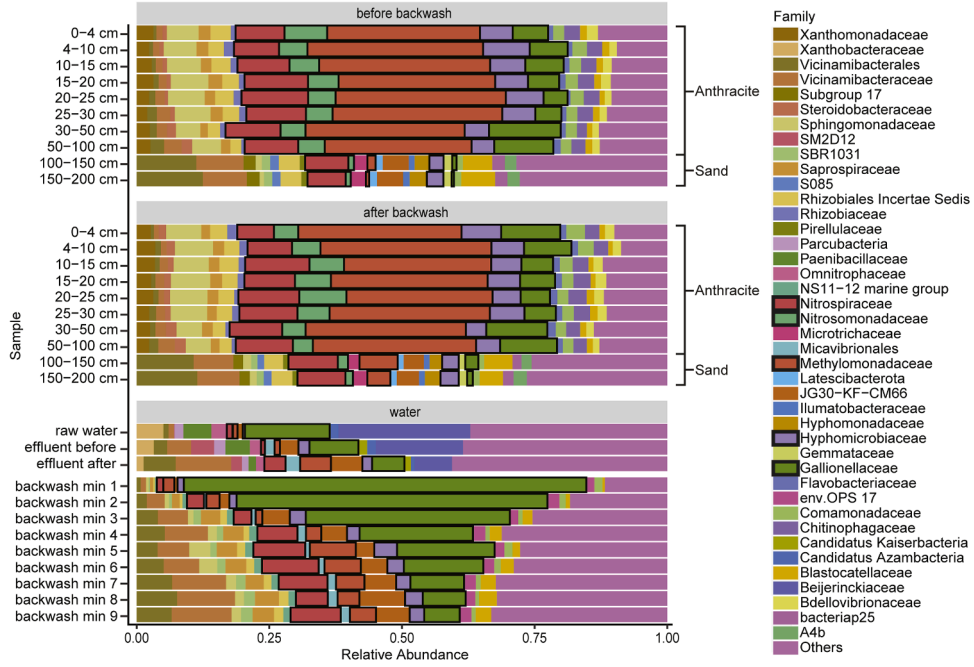

Fig. 3. Microbial community composition of filter medium and water samples. The microbial community composition was determined by 16S rRNA gene amplicon sequencing. Samples were taken in June 2021 before (after 136 h of runtime) and 2 h after backwash, and water samples were taken from the raw water, effluent water (before and after backwash), and the backwash water during the backwashing event. Only families with relative abundances > 1% are shown. The families *Nitrospiraceae, Nitrosomonadaceae, Methylomonadaceae, Hyphomicrobiaceae*, and *Gallionellaceae* are highlighted.

Table 2
Relative abundance of the main genera in the most abundant families as determined by 16S rRNA gene amplicon sequencing. The runtime of the filter at the time of sampling and the sample type are given. Samples were taken in June 2021. A, anthracite; S, sand.

Family	Genus	136 h		2 h		raw water	effluent		back-wash
		A	S	A	S		2 h	136 h	
Methylomonadaceae	*Methyloglobulus*	82%	84%	83%	89%	80%	96%	80%	86%
	Crenothrix	16%	13%	15%	10%	9%	3%	18%	12%
Nitrospiraceae	*Nitrospira*	100%	100%	100 %	100%	100%	100%	100%	100%
Nitrosomonadaceae	*Nitrosomonas*	98%	27%	99%	65%	25%	54%	29%	91%
Gallionellaceae	*Gallionella*	77%	96%	75%	76%	97%	96%	97%	97%
	Candidatus Nitrotoga	21%	4%	23%	24%	2%	3%	2%	2%
Hyphomicrobiaceae	*Hyphomicrobiaceae*	86%	37%	86%	44%	72%	53%	22%	64%
	Pedomicrobium	9%	38%	9%	36%	22%	32%	53%	23%
Sphingomonadaceae	*Novosphingobium*	68%	80%	68%	76%	63%	49%	53%	62%
	Spingorhabdus	17%	2%	16%	7%	11%	8%	0%	13%

nitrifying community of the anthracite harbored the families *Nitrospiraceae* (7–13%) and *Nitrosomadaceae* (4–9%). While the *Methylomonadaceae, Gallionellaceae,* and *Nitrosomonadaceae* were less abundant in the sand (1–7%, 0–2% and 1–2%, respectively) compared to the anthracite layer, the relative abundance of *Nitrospiraceae* remained high also in the sand layer (7–9%).

The microbial community of the raw water, which acts as the inoculum of the filter, was dominated by members of the families *Beijerinckiaceae* (24%) and *Gallionellaceae* (16%), followed by *Paenibacillaceae* (5%) and *Xanthobacteraceae* (5%; Fig. 3). This was notably different from the microbial community of the filter medium, which indicates that the change in O_2 concentrations after plate aeration as well as the possibility of attachment to the filter medium selectively enriches for certain groups of bacteria, as was observed before (Gülay et al., 2016). Except for the *Gallionellaceae*, other bacterial groups that likely play a role in Fe, Mn, and NH_4^+ removal (e.g., *Nitrospiraceae, Nitrosomonadacecae, Hyphomicrobiaceae*) had low relative abundances in the raw water compared to the filter medium (Fig. 3).

The microbial composition in the effluent water differed noticeably from both the raw water and the filter medium, yet it exhibited a closer resemblance to the microbial community found in the raw water, at least towards the end of the filter runtime. However, the total bacterial number in the effluent water was higher compared to the raw water (5.7×10^6 - 1.3×10^7 and 6.0×10^5 16S rRNA gene copies L^{-1}, respectively; Fig. 4), which is likely caused by the detachment of bacteria from the filter medium. This is in agreement with previous work (Dott and Trampisch, 1983) that found higher colony counts in effluent water of an RSF compared to the raw water. The microbial community of the effluent water after 136 h of filter operation was characterized by a high abundance of *Beijerinckiaceae* (16%), *Vicinamibacteraceae* (9%), and *Gallionellaceae* (5%; Fig. 3), the latter containing almost exclusively members of the genus *Gallionella* (Table 2). This indicates that the raw water microbial community had the largest influence on the effluent and the incoming bacterial biomass was not completely removed by the filter medium. The observed increased quantity of bacteria in the effluent compared to the raw water likely was due to a combination of proliferation of the incoming microorganisms in the filter and washout of the filter medium community (Fig. 4). This contrasts with research from Pinto et al. (2012), who found that the microbial community of the filter effluent was more similar to the filter medium than to the source water. However, in that study, a mixture of surface and groundwater was used as the source water, necessitating additional treatment steps, such as flocculation, sedimentation, and ozonation before rapid sand filtration. As ozonation kills almost all bacteria, this explains why the microbial community of the effluent resembled the filter medium rather than the raw water (Pinto et al., 2012). Interestingly, we observed here that the microbial community in the effluent water 2 h after backwash resembles a mixture of the microbial communities present in the raw water and the different layers of filter medium, indicating that backwashing dislodges parts of the microbial biomass, which is not completely removed yet during the backwash (see below; Fig. 3).

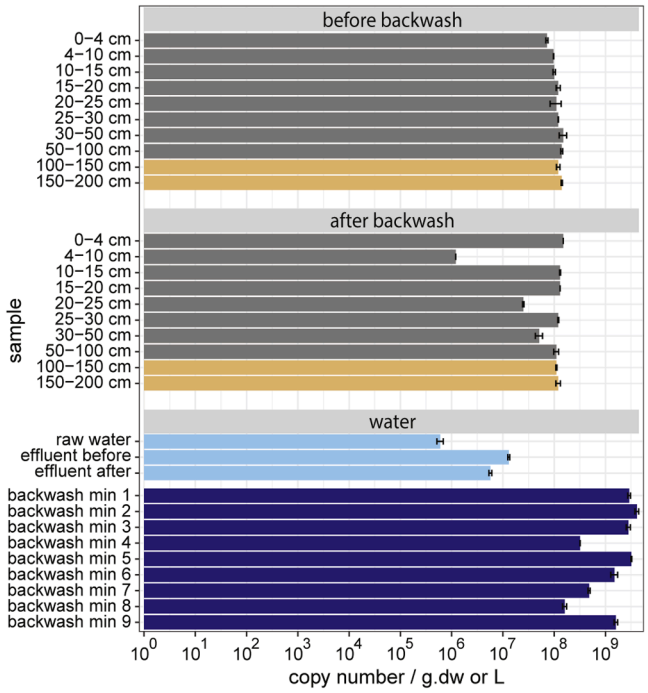

Fig. 4. Absolute bacterial abundances of filter medium and water samples. Absolute abundances were determined by qPCR for the filter medium before and after backwashing, the raw water, effluent water before and after backwashing, and backwash water. Samples before and after backwashing were taken in June 2021 at 136 h and 2 h runtime, respectively. The error bars represent the standard deviation of technical duplicates.

3.2. Filter function before backwashing

The filter had been running for 72 h in March 2021 and 48 h in October 2021 before it was backwashed, corresponding to a loading of ~34 and 43 kg Fe, and ~1.68 and 2.07 kg Mn onto the filter, respectively (Table 1). This accumulation was reflected in high concentrations of particulate Fe (~400 μM) in the supernatant (Fig. 1) and although most Fe^{2+} was removed in the anthracite layer, Fe^{2+} also reached the underlying sand layer in March (Fig. 1). At this time, a breakthrough of iron flocs (~140 μM) was also observed.

Especially NH_4^+ removal moved deeper into the sand layer over time

(Fig. 2), as also observed at other DWTPs (Corbera-Rubio et al., 2024; De Vet et al., 2009). The role of Fe flocs in inhibiting nitrification remains elusive (Corbera-Rubio et al., 2024). Fe is a known scavenger for dissolved phosphorus (Romano et al., 2017) and metals such as copper (Jackson and Bistricki, 1995), which both can be important for efficient nitrification in rapid sand filters (De Vet et al., 2012; Wagner et al., 2016). However, a limiting role of P is unlikely, given its presence in the anthracite, and in the upper part of the sand layer where nitrification also occurred (Supplementary data). Floc buildup reduces pore space and can lead to higher water velocities. However, porous flow modeling of rapid sand filtration suggests that increased flowrates alone cannot explain the delayed nitrification (Corbera-Rubio et al., 2024)

The overall removal efficiencies of Mn^{2+} (~80%) did not differ substantially before and after backwash (Fig. 1). However, recent work has shown that Fe^{2+} can efficiently inhibit biological Mn^{2+} oxidation, as Fe^{2+} can attach to the cell surface and damage the cell membrane of *Pseudomonas putida* MnB1 (Tong et al., 2022). Therefore, if microbiological processes contribute to Mn^{2+} removal, as is the case in the dual-media filter studied here (Haukelidsaeter et al., 2023), it is beneficial to separate the removal of Fe and Mn in the filtration process. The anthracite, which is characterized by large particles and high porosity, efficiently removes Fe from the water through physical straining of the flocs combined with heterogeneous and biological removal processes. The sand, in turn, is characterized by metal coatings harboring a distinct diverse microbial community that is capable of removing Mn and NH_4^+ through biological oxidation and, in the case of Mn, potentially also facilitating heterogeneous oxidation (Haukelidsaeter et al., 2024). While some separation of Fe and Mn removal is also observed in single media filters (Haukelidsaeter et al., 2024), it is more pronounced in dual-media filters, illustrating the value of using the latter for separating removal processes.

Turbidity measurements from a similar backwash cycle showed an increase in turbidity before backwash (Fig. 5). This increase in turbidity can be attributed to the breakthrough of iron flocs to the effluent, which may be linked to preferential flow in the filter, i.e., zones of high or low flow (Haukelidsaeter et al., 2023). Preferential flow can be more important in rapid sand filters with increased deposition of flocs to the filter because these oxides can create channels or pathways that allow water to flow more easily through certain areas of the filter, bypassing the intended filtration process. Consequently, the contact time between the water and the filter media may not be sufficient for the effective removal of Fe, Mn, and NH_4^+, moving the processes to greater depth in the filter.

The microbial community growing on the filter medium did not change much over the runtime of a filter (Fig. 3 and Supplementary Figure S3), and only minimal changes were observed in the total number of bacteria present (Fig. 4). Still, the total bacterial numbers in the effluent were highest just before backwash. Interestingly, a slight increase in the relative abundance of *Gallionellaceae* was observed with increasing filter runtime in March (Supplementary Figure S3), but not in June.

3.3. Backwash

The backwash water contained two visually distinct types of particles. The majority of these had a fluffy appearance and consisted mostly of Fe oxides with some Mn oxides, likely corresponding to the Fe flocs removed by backwash (Supplementary Figure S4). Additionally, angular particles consisting solely of Fe, which likely represent fragments of the Fe coating from the anthracite layer, were observed (Supplementary Figure S5). However, as most Mn is removed through chemical and/or biological oxidation in contact with the filter medium coating, less Mn was removed by backwashing, as also seen in single media filters (Haukelidsaeter et al., 2024). As filters age, the amount of Fe and Mn coating on the anthracite and sand, respectively, increases (Haukelidsaeter et al., 2023), supporting that the amount of Fe and Mn bound to the filter exceeds their quantity lost during backwashing.

During the first minutes of the backwash cycle, the backwash water was dominated by members of the *Gallionellaceae* (up to 76%), which were almost completely made up of the genus *Gallionella.* While not to the magnitude observed here, the presence of *Gallionella* in the backwash water of rapid dual-media filters has been described before (van Beek et al., 2012). It was hypothesized that their washout would result in reduced bacterial Fe oxidation after backwash, which we cannot verify here, as the contribution of biological Fe oxidation was not quantified. As the backwash procedure continued, *Gallionella* became relatively less abundant in the backwash water, whereas bacteria belonging to the order *Vicinamibacterales* increased in relative abundance (Fig. 3). Towards the end of the backwash cycle, the microbial community of the backwash water mostly resembled that of the sand layer, as shown by NMDS analysis on beta diversity (Fig. 6). This indicates that while *Gallionella* spp. are preferentially washed out during the beginning of the backwash cycle, the air scouring generally affects the microbial community of the sand more than of the anthracite layer. One reason for this could be the sand layer's closer proximity to the air scouring source, resulting in more pronounced effects. Additionally, sand is denser than anthracite, requiring more force to displace and allowing air to pass through, possibly generating higher shear forces than the lighter anthracite.

The highest total bacterial numbers in the backwash water were observed at the beginning of the backwash cycle, and there seems to be a decline four minutes into the backwash cycle (Fig. 4). After five minutes of air scouring, the number of bacteria in the backwash water increased again, with a subsequent steady decline during the last part of the backwash procedure, except for the last sample.

3.4. Filter function after backwashing

Patches of dense orange-red Fe oxides had settled on the filter bed surface over the anthracite at several locations (Supplementary

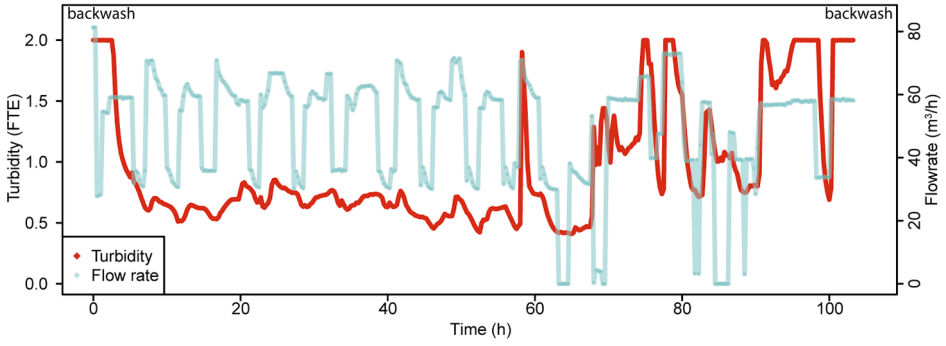

Fig. 5. Effluent turbidity determination. Turbidity (FTE) of the effluent (red) and flow rate (light blue) between two backwash events. Measurements were performed in January 2023.

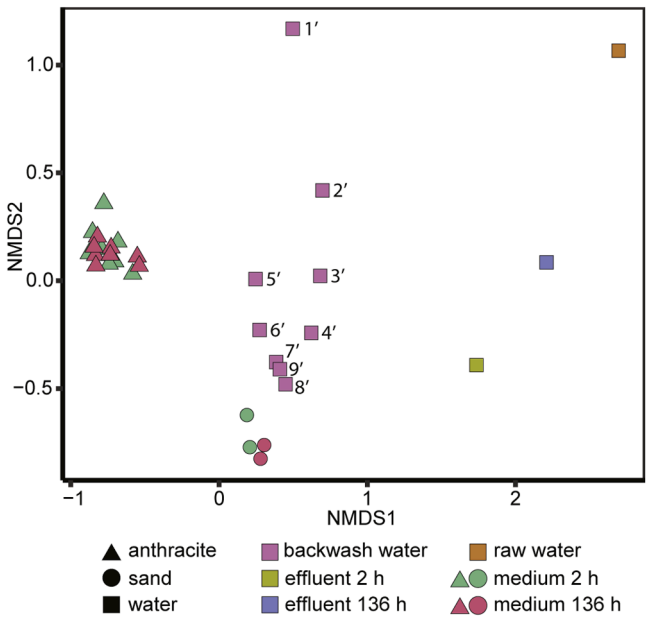

Fig. 6. NMDS analysis on the beta diversity of the microbial communities. Beta diversity was calculated as Bray-Curtis dissimilarity for the filter medium and water samples, based on 16S rRNA gene amplicon sequencing data. Samples were taken in June 2021.

Figure S6). These patches may hinder uniform water flow through the filter bed, disrupting hydraulic gradients and causing irregular flow patterns, even post-backwash.

Following backwash, a decrease in particulate Fe concentrations in the anthracite layer was noted, although 5.9–8.2 μM of particulate Fe still broke through to the effluent (Fig. 1). This observation is further supported by the increased turbidity observed after backwashing of the filter (Fig. 5). The breakthrough of Fe can be attributed to settling processes post-backwash, allowing dislodged coatings, biomass, or Fe flocs to pass through the filter more easily.

Moreover, post-backwash, removal of dissolved Fe, Mn, and NH_4^+ was observed higher in the filter, indicating reversible inhibition by Fe oxides and restoration of pre-backwash filtration function, as also recently reported elsewhere (Corbera-Rubio et al., 2024). The peak Fe removal efficiency occurred 24 h post-backwash, coinciding with notably low turbidity levels in the effluent, suggesting the need for settling time and indicating a duration required for the microbial community to become fully active post-backwash (Fig. 5).

The microbial community composition of the filter medium remained largely unchanged by backwashing (Fig. 3, Supplementary Figure S3). An exception was the decrease in the relative abundance of *Gallionellaceae* in March 2021 after backwashing (Supplementary Figure S3), which largely recovered after 24 h. While this decrease in *Gallionellaceae* was not observed during the June sampling, members of the genus *Gallionella* were highly abundant in the backwash water. This, in addition to the decrease in *Gallionella* in the filter medium after backwashing, indicates that *Gallionella* are preferentially washed out from the filter (Fig. 3). This decrease has recently also been observed at a different DWTP using single media filtration (Haukelidsaeter et al., 2024). However, since dual-media filtration is often employed to treat groundwater with high Fe concentrations, studying the effects of backwashing on Fe-oxidizing bacteria in dual-media filters remains of special interest. In both March and in June, there was a notable increase in the relative contribution of *Gallionella* within the *Gallionellaceae*, particularly in the sand layer (Table 2, Supplementary Table S1). Together with the fact that the relative abundance of *Gallionellaceae* remains stable as filters age (Haukelidsaeter et al., 2023), this suggests that *Gallionella* spp. grow faster than members of other bacterial genera during filter operation. Due to such enhanced growth, freshly formed biomass of these organisms might be less well attached to the filter medium and might grow attached to Fe flocs that are removed during backwash. Generally, however, despite an apparent loss of bacteria as evidenced by the quantity of bacteria in the backwash water, the absolute abundance of bacteria in the filter medium was not reduced by backwashing (Fig. 4). Additionally, the overall microbial community structures of the anthracite and sand layers remained largely unchanged (Fig. 6), indicating that the backwashing procedure had a minimal influence on the microbial community.

Contrastingly, the microbial community composition of the effluent water was different 2 h after backwashing compared to before. While the same three families, *Vicinamibacteraceae, Beijerinckiaceae,* and *Gallionellaceae,* were the most abundant families at both sampling time points, their relative abundances changed from 4.5%, 16.3%, and 9.1% to 10.4%, 7.1%, and 6.1%, respectively. Moreover, 2 h after backwashing, the microbial community of the effluent was more similar to the filter medium, while it rather resembled the raw water before (Figs. 3 and 5). This indicates release of bacteria from the sand layer to the effluent right after backwashing. However, the observed total bacterial abundances in the effluent water were lower after backwashing compared to before.

The anthracite and sand layers of the dual-media rapid sand filter contained distinct microbial communities that remained largely unchanged by backwashing, as also previously described (Ramsay et al., 2021; Corbera-Rubio et al., 2023). This is consistent with visual observations of the filter medium right after backwashing and confirms that these layers do not get mixed by backwashing. This is likely the case because any mixing that might occur during backwashing is restored in a final water-washing step, where flow is gradually reduced to restore the separation of anthracite and sand. Each filter medium layer contained homogeneous microbial communities (Fig. 3, Supplementary Figure S3), achieved by separating removal processes using filter media of different densities that ensure that the microbes involved in these processes remain in their respective locations after cleaning procedures. In single media filters, stratification of the microbial community has also been observed despite regular backwash, which was linked to the continuous success of the filter (Haukelidsaeter et al., 2024).

3.5. Implications for drinking water treatment

Our findings highlight several key considerations for drinking water treatment. Regular inspection and maintenance of filters after backwashing are essential to prevent issues such as clogging, channeling, and preferential flow. The turbidity sensor installed in November 2022 demonstrated that a robust monitoring system continuously measuring turbidity can help detect irregularities in filter performance, allowing for prompt corrective actions. These actions may include adjusting backwashing frequency, replacing the filter medium (anthracite or sand), or performing periodic surface cleaning to maintain optimal filtration performance.

Drinking water companies should also carefully assess the duration and intensity of backwashing. First, filters may currently be washed for longer than necessary, leading to excessive loss of pre-filtrate water and increased energy consumption. Installing turbidity sensors to monitor Fe flocs in the backwash water could help determine when the filter has been sufficiently cleaned, reducing waste and energy use. Second, while our results show that intensive backwashing, including air scouring, minimally affects the mineral coating and microbial community, it may still be beneficial for water companies to explore milder backwashing programs. Milder backwashing would not only reduce energy consumption but also promote the development of specialized zones within the filter bed, fostering microbial communities adapted to the specific contaminants encountered at different depths, which has been shown to be advantageous in single-media filters (Haukelidsaeter et al., 2024). In the dual-media filters we studied, two distinct microbial communities associate with the anthracite and sand layers that, however, are

homogenous across the respective layers due to backwashing. This demonstrates the value of dual-media filtration, allowing for process separation despite aggressive backwashing. However, further research should explore whether milder backwashing could enhance microbial specialization also in dual-media filters.

4. Conclusions

In this study, we showed how backwashing is crucial for maintaining efficient removal of Fe, Mn, and NH_4^+ in rapid sand filters. The accumulation of metal oxides in the filter, primarily in the form of Fe flocs, caused a breakthrough of Fe flocs and moved nitrification and Fe and Mn oxidation deeper into the filter. Backwashing mainly restored filter function by removing these Fe flocs, and preferentially washed out *Gallionella*. While the microbial community composition was minimally impacted, temporary effects post-backwash included increased Fe leakage and higher turbidity in the effluent of the filter in the first hours after start-up due to slow settlement of the filter medium.

The filter media selection at the DWTP separates metal oxide removal processes to a higher degree than in single media filters, with Fe removal primarily occurring in the anthracite and Mn removal in the sand layer. Biological nitrification could take place throughout the filter, as key nitrifiers were abundant in both the anthracite and sand layers. The individual layers largely mixed internally, resulting in a homogeneous microbial community in the anthracite and sand layers, respectively. Given the variability in operating conditions and groundwater chemistries, caution is needed when extrapolating results from one drinking water production site to others. Nonetheless, the findings presented here are broadly applicable to other locations utilizing dual-media rapid sand filters for treating anoxic groundwater with high levels of methane, iron, ammonium, and manganese. To advance our understanding of rapid sand filtration, future research should prioritize a careful selection of diverse operating conditions and groundwater chemistries to identify general and site-specific parameters that allow for predicting filter function. Finally, despite occasional breakthroughs of Fe and Mn from the filters, subsequent treatment steps at the DWTP ensured compliance with drinking water standards.

CRediT authorship contribution statement

Alje S. Boersma: Writing – original draft, Visualization, Investigation, Data curation, Conceptualization. **Signe Haukelidsaeter:** Writing – original draft, Visualization, Investigation, Data curation, Conceptualization. **Liam Kirwan:** Investigation. **Alessia Corbetta:** Investigation. **Luuk Vos:** Investigation. **Wytze K. Lenstra:** Investigation. **Frank Schoonenberg:** Resources. **Karl Borger:** Investigation. **Paul W.J.J. van der Wielen:** Writing – review & editing, Supervision, Conceptualization. **Maartje A.H.J. van Kessel:** Writing – review & editing, Supervision, Project administration, Conceptualization. **Caroline P. Slomp:** Writing – review & editing, Supervision, Project administration, Funding acquisition, Conceptualization. **Sebastian Lücker:** Writing – review & editing, Supervision, Project administration, Funding acquisition, Conceptualization.

Declaration of competing interest

The authors declare that they have no known competing financial interests or personal relationships that could have appeared to influence the work reported in this paper.

Acknowledgments

We are grateful to H. Doeve, M. Pipping, and Vitens N.V. for their support and collaboration during the visits to the drinking water treatment plants. We also thank L. Piso, N. van Helmond, J. Visser, E. Hellebrand, and J. Mulder, and K. Pelsma for analytical support, and T. Marcus for graphical design. This research was funded by the Netherlands Organisation for Scientific Research (NWO) partnership program Dunea–Vitens: Sand Filtration (grant 17841). MAHJvK and SL were funded by NWO (016.Veni.192.062 and 016.Vidi.189.050, respectively), CPS by the European Research Council (ERC Synergy Grant 694407 MARIX).

Supplementary materials

Supplementary material associated with this article can be found, in the online version, at doi:10.1016/j.watres.2024.122809.

Data availability

Sequencing data has been deposited in the NCBI Sequencing Read Archive (SRA) under BioProject PRJNA1107137

BioProject PRJNA1107137 (Original data) https://www.ncbi.nlm.nih.gov/bioproject/?term=PRJNA1107137 (NCBI SRA).

References

Albers, C.N., Ellegaard-Jensen, L., Harder, C.B., Rosendahl, S., Knudsen, B.E., Ekelund, F., Aamand, J., 2014. Groundwater chemistry determines the prokaryotic community structure of waterworks sand filters. https://doi.org/10.1021/es5046452.

Beshr, S., Moustafa, M., Fayed, M., Aly, S., 2023. Evaluation of water consumption in rapid sand filters backwashed under varied physical conditions. Alexandr. Eng. J. 64, 601–613. https://doi.org/10.1016/J.AEJ.2022.08.048.

Bourke, N., Carty, G., Crowe, M., Lambert, M., 1995. Water treatment manuals: filtration. Environ. Protect. Agency.

Bruins, J.H., Petrusevski, B., Slokar, Y.M., Wübbels, G.H., Huysman, K., Wullings, B.A., Joris, K., Kruithof, J.C., Kennedy, M.D., 2017. Identification of the bacterial population in manganese removal filters. Water Supply 17 (3), 842–850. https://doi.org/10.2166/WS.2016.184.

Callahan, B.J., McMurdie, P.J., Rosen, M.J., Han, A.W., Johnson, A.J.A., Holmes, S.P., 2016. DADA2: high-resolution sample inference from Illumina amplicon data. Nat. Methods 13 (7), 581–583. https://doi.org/10.1038/nMeth.3869.

Caporaso, J.G., Lauber, C.L., Walters, W.A., Berg-Lyons, D., Huntley, J., Fierer, N., Owens, S.M., Betley, J., Fraser, L., Bauer, M., Gormley, N., Gilbert, J.A., Smith, G., Knight, R., 2012. Ultra-high-throughput microbial community analysis on the Illumina HiSeq and MiSeq platforms. ISMe J. 6 (8), 1621–1624. https://doi.org/10.1038/ISMEJ.2012.8.

Claff, S.R., Sullivan, L.A., Burton, E.D., Bush, R.T., 2010. A sequential extraction procedure for acid sulfate soils: partitioning of iron. Geoderma 155 (3–4), 224–230. https://doi.org/10.1016/J.GEODERMA.2009.12.002.

Corbera-Rubio, F., Kruisdijk, E., Malheiro, S., Leblond, M., Verschoor, L., van Loosdrecht, M.C.M., Laureni, M., van Halem, D., 2024. A difficult coexistence: resolving the iron-induced nitrification delay in groundwater filters. Water Res 260, 121923. https://doi.org/10.1016/j.watres.2024.121923.

Corbera-Rubio, F., Laureni, M., Koudijs, N., Müller, S., van Alen, T., Schoonenberg, F., Lücker, S., Pabst, M., van Loosdrecht, M.C.M., van Halem, D., 2023. Meta-omics profiling of full-scale groundwater rapid sand filters explains stratification of iron, ammonium and manganese removals. Water Res. 233, 119805. https://doi.org/10.1016/J.WATRES.2023.119805.

Daims, H., Lebedeva, E.V., Pjevac, P., Han, P., Herbold, C., Albertsen, M., Jehmlich, N., Palatinszky, M., Vierheilig, J., Bulaev, A., Kirkegaard, R.H., Von Bergen, M., Rattei, T., Bendinger, B., Nielsen, H., Wagner, M., 2015. Complete nitrification by *Nitrospira* bacteria. Nature 528, 504–509. https://doi.org/10.1038/nature16461.

de Vet, W.W.J.M., Dinkla, I.J.T., Rietveld, L.C., van Loosdrecht, M.C.M, 2011. Biological iron oxidation by Gallionella spp. in drinking water production under fully aerated conditions. Water Res. 45 (17), 5389–5398. https://doi.org/10.1016/j.watres.2011.07.028.

de Vet, W.W.J.M., Rietveld, L.C., van Loosdrecht, M.C.M., 2009. Influence of iron on nitrification in full-scale drinking water trickling filters. J. Water Supply: Res. Technol. - AQUA 58 (4), 247–256. https://doi.org/10.2166/aqua.2009.115.

de Vet, W.W.J.M., van Loosdrecht, M.C.M., Rietveld, L.C., 2012. Phosphorus limitation in nitrifying groundwater filters. Water Res. 46 (4), 1061–1069. https://doi.org/10.1016/J.WATRES.2011.11.075.

Dott, W., Trampisch, H.J., 1983. Qualitative und Quantitative Bestimmung von Bakterienpopulationen aus aquatischen Biotopen. 5. Mitteilung: vergleichende Untersuchungen an zwei Schnellsandfiltern. Zentralbl. Bakteriol. Mikrobiol. Hyg. - Abt. 1 Orig. B. Hyg. 174 (1–2), 174–181.

Fleming, E.J., Woyke, T., Donatello, R.A., Kuypers, M.M.M., Sczyrba, A., Littmann, S., Emerson, D., 2018. Insights into the fundamental physiology of the uncultured Fe-oxidizing bacterium *Leptothrix ochracea*. Appl. Environ. Microbiol. 84 (9), e0223917. https://doi.org/10.1128/AEM.02239-17.

Gude, J.C.J., Joris, K., Huysman, K., Rietveld, L.C., van Halem, D., 2018. Effect of supernatant water level on As removal in biological rapid sand filters. Water. Res. X. 1, 100013. https://doi.org/10.1016/J.WROA.2018.100013.

Gülay, A., Çekiç, Y., Musovic, S., Albrechtsen, H.J., Smets, B.F., 2018. Diversity of iron oxidizers in groundwater-fed rapid sand filters: evidence of Fe(II)-dependent growth by *Curvibacter* and *Undibacterium* spp. Front. Microbiol. 9, 2808. https://doi.org/10.3389/FMICB.2018.02808.

Gülay, A., Musovic, S., Albrechtsen, H.J., Smets, B.F., 2013. Neutrophilic iron-oxidizing bacteria: occurrence and relevance in biological drinking water treatment. Water Supply 13 (5), 1295–1301. https://doi.org/10.2166/WS.2013.113.

Gülay, A., Musovic, S., Albrechtsen, H.-J., Al-Soud, W.A., Sørensen, S.J., Smets, B.F., 2016. Ecological patterns, diversity and core taxa of microbial communities in groundwater-fed rapid gravity filters. ISME J. 10, 2209–2222. https://doi.org/10.1038/ismej.2016.16.

Haukelidsaeter, S., Boersma, A.S., Kirwan, L., Corbetta, A., Gorres, I.D., Lenstra, W.K., Schoonenberg, F.K., Borger, K., Vos, L., van der Wielen, P.W.J.J., van Kessel, M.A.H. J., Lücker, S., Slomp, C.P., 2023. Influence of filter age on Fe, Mn and NH^{4+} removal in dual-media rapid sand filters used for drinking water production. Water Res. 242, 120184. https://doi.org/10.1016/J.WATRES.2023.120184.

Haukelidsaeter, S., Boersma, A.S., Piso, L., Lenstra, W.K., van Helmond, N.A.G.M., Schoonenberg, F., van der Pol, E., Hurtarte, L.C.C., van der Wielen, P.W.J.J., Behrends, T., van Kessel, M.A.H.J., Lücker, S., Slomp, C.P, 2024. Efficient chemical and microbial removal of iron and manganese in a rapid sand filter and impact of regular backwash. Appl. Geochem. 162, 105904. https://doi.org/10.1016/j.apgeochem.2024.105904.

Herlemann, D.P.R., Labrenz, M., Jürgens, K., Bertilsson, S., Waniek, J.J., Andersson, A.F., 2011. Transitions in bacterial communities along the 2000 km salinity gradient of the Baltic Sea. ISME J. 5 (10), 1571–1579. https://doi.org/10.1038/ISMEJ.2011.41.

Hu, W., Liang, J., Ju, F., Wang, Q., Liu, R., Bai, Y., Liu, H., Qu, J., 2020. Metagenomics unravels differential microbiome composition and metabolic potential in rapid sand filters purifying surface water versus groundwater. Environ. Sci. Technol 54, 5206. https://doi.org/10.1021/acs.est.9b07143.

Jackson, T.A., Bistricki, T., 1995. Selective scavenging of copper, zinc, lead, and arsenic by iron and manganese oxyhydroxide coatings on plankton in lakes polluted with mine and smelter wastes: results of energy dispersive X-ray micro-analysis. J. Geochem. Explor. 52 (1–2), 97–125. https://doi.org/10.1016/0375-6742(94)00027-9.

Jumppanen, T., Jokinen, M., Airo, J., Klemm, M., Hoger, D., Suoniemi-Kähärä, A.. Automated total oxidized nitrogen method using vanadium as reductant with correlation to cadmium and hydrazine reductant methods in sea, natural, and waste waters. Thermo Fisher Sci. https://assets.thermofisher.com/TFS-Assets/CMD/Application-Notes/an-71395-da-ton-vanadium-an71395-en.pdf.

Larsen, E.I., Sly, L.I., McEwan, A.G., 1999. Manganese (II) adsorption and oxidation by whole cells and a membrane fraction of Pedomicrobium sp. ACM 3067. Arch. Microbiol. 171, 257–264. https://doi.org/10.1007/s002030050708.

Lenstra, W.K., Klomp, R., Molema, F., Behrends, T., Slomp, C.P., 2021. A sequential extraction procedure for particulate manganese and its application to coastal marine sediments. Chem. Geol. 584, 120538. https://doi.org/10.1016/J.CHEMGEO.2021.120538.

Marcus, D.N., Pinto, A., Anantharaman, K., Ruberg, S.A., Kramer, E.L., Raskin, L., Dick, G.J., 2017. Diverse manganese(II)-oxidizing bacteria are prevalent in drinking water systems. Environ. Microbiol. Rep. 9 (2), 120–128. https://doi.org/10.1111/1758-2229.12508.

McMurdie, P.J., Holmes, S., 2013. Phyloseq: an R package for reproducible interactive analysis and graphics of microbiome census data. PLoS. One 8 (4). https://doi.org/10.1371/journal.pone.0061217.

Müller, S., Corbera-Rubio, F., Kegel, F.S., Laureni, M., van Loosdrecht, M.C., van Halem, D., 2024. Shifting to biology promotes highly efficient iron removal in groundwater filters. Water Res. 262, 122–135. https://doi.org/10.1101/2024.02.14.580244.

Muyzer, G., De Waal, E.C., Uitterlinden, A.G., 1993. Profiling of complex microbial populations by denaturing gradient gel electrophoresis analysis of polymerase chain reaction-amplified genes coding for 16S rRNA. Appl. Environ. Microbiol. 59 (3), 695–700. https://doi.org/10.1128/AEM.59.3.695-700.1993.

Nadkarni, M.A., Martin, F.E., Jacques, N.A., Hunter, N., 2002. Determination of bacterial load by real-time PCR using a broad-range (universal) probe and primers set. Microbiology 148 (1), 257–266. https://doi.org/10.1099/00221287-148-1-257.

Nitzsche, K.S., Weigold, P., Lösekann-Behrens, T., Kappler, A., Behrens, S., 2015. Microbial community composition of a household sand filter used for arsenic, iron, and manganese removal from groundwater in Vietnam. Chemosphere 138, 47–59. https://doi.org/10.1016/j.chemosphere.2015.05.032.

Palermo, C., Dittrich, M., 2016. Evidence for the biogenic origin of manganese-enriched layers in Lake Superior sediments. Environ. Microbiol. Rep. 8 (2), 179–186. https://doi.org/10.1111/1758-2229.12364.

Palomo, A., Fowler, J., Gülay, A., Rasmussen, S., Sicheritz-Ponten, T., Smets, B.F., 2016. Metagenomic analysis of rapid gravity sand filter microbial communities suggests novel physiology of *Nitrospira* spp. ISME J. 10, 2569–2581. https://doi.org/10.1038/ismej.2016.63.

Pinto, A.J., Xi, C., Raskin, L., 2012. Bacterial community structure in the drinking water microbiome is governed by filtration processes. Environ. Sci. Technol. 46 (16), 8851–8859. https://doi.org/10.1021/es302042t.

Poghosyan, L., Koch, H., Frank, J., van Kessel, M.A.H.J., Cremers, G., van Alen, T., Jetten, M.S.M., Op den Camp, H.J.M., Lücker, S., 2020. Metagenomic profiling of ammonia- and methane-oxidizing microorganisms in two sequential rapid sand filters. Water Res. 185. https://doi.org/10.1016/j.watres.2020.116288.

Quast, C., Pruesse, E., Yilmaz, P., Gerken, J., Schweer, T., Yarza, P., Peplies, J., Glöckner, F.O., 2013. The SILVA ribosomal RNA gene database project: improved data processing and web-based tools. Nucleic Acids Res. 41 (D1), D590–D596 doi:10.1093/nar/gks1219.

R Core Team, 2021. R: a language and environment for statistical computing. R Foundation for Statistical Computing. Vienna, Austria. URL. https://www.R-project.org/.

Ramsay, L., Du, F., Lund, M., He, H., Søborg, D.A., 2021. Grain displacement during backwash of drinking water filters. Water Supply 21 (1), 356–367. https://doi.org/10.2166/WS.2020.300.

Romano, S., Bondarev, V., Kölling, M., Dittmar, T., Schulz-Vogt, H.N., 2017. Phosphate limitation triggers the dissolution of precipitated iron by the marine bacterium *Pseudovibrio* sp. FO-BEG1. Front. Microbiol. 8 (MAR), 235101. https://doi.org/10.3389/FMICB.2017.00364/BIBTEX.

Sung, W., Morgan, J.J., 1980. Kinetics and product of ferrous iron oxygenation in aqueous systems. Am. Chem. Soc. 14 (5), 561. https://doi.org/10.1021/es60165a006.

Tong, M., Zhao, Y., Sun, Q., Li, P., Liu, H., Yuan, S., 2022. Fe(II) oxygenation inhibits bacterial Mn(II) oxidation by P. putida MnB1 in groundwater under O_2-perturbed conditions. J. Hazard. Mater. 435, 128972. https://doi.org/10.1016/J.JHAZMAT.2022.128972.

van Beek, C.G.E.M., Dusseldorp, J., Joris, K., Huysman, K., Leijssen, H., Schoonenberg Kegel, F., de Vet, W.W.J.M, van de Wetering, S., Hofs, B, 2016. Contributions of homogeneous, heterogeneous and biological iron(II) oxidation in aeration and rapid sand filtration (RSF) in field sites. J. Water Supply: Res. Technol.-AQUA 65 (3), 195–207. https://doi.org/10.2166/aqua.2015.059.

van Beek, C.G.E.M., Hiemstra, T., Hofs, B., Nederlof, M.M., van Paassen, J.A.M., Reijnen, G.K., 2012. Homogeneous, heterogeneous and biological oxidation of iron (II) in rapid sand filtration. J. Water Supply: Res. Technol.-AQUA 61 (1), 1–13. https://doi.org/10.2166/AQUA.2012.033.

van der Gun, J. (2012). The United Nations world water development report: groundwater and global change: trends, opportunities and challenges. https://unesdoc.unesco.org/ark:/48223/pf0000215496.

van Kessel, M.A.H.J., Speth, D.R., Albertsen, M., Nielsen, P.H., Op den Camp, H.J.M., Kartal, B., Jetten, M.S.M., Lücker, S., 2015. Complete nitrification by a single microorganism. Nature 528 (7583), 555–559. https://doi.org/10.1038/nature16459.

Vries, D., Bertelkamp, C., Schoonenberg Kegel, F., Hofs, B., Dusseldorp, J., Bruins, J.H., de Vet, W., van den Akker, B., 2017. Iron and manganese removal: recent advances in modelling treatment efficiency by rapid sand filtration. Water Res. 109, 35–45. https://doi.org/10.1016/j.watres.2016.11.032.

Wagner, F.B., Nielsen, P.B., Boe-Hansen, R., Albrechtsen, H.J., 2016. Copper deficiency can limit nitrification in biological rapid sand filters for drinking water production. Water Res. 95, 280–288. https://doi.org/10.1016/j.watres.2016.03.025.